Theory of the collective behavior of two-dimensional periodic ensembles of dipole-coupled magnetic nanoparticles

David Gallina [*] and G. M. Pastor
Institut für Theoretische Physik, Universität Kassel, Heinrich-Plett-Straße 40, 34132 Kassel, Germany

The magnetic behavior of two-dimensional (2D) periodic ensembles of dipole-coupled nanoparticles (NPs) is investigated theoretically by considering all possible structural organizations in 2D Bravais lattices, namely, square, triangular, rectangular, rhombic, and oblique lattices. The different interaction-energy landscapes (ELs) are characterized by determining the local minima that define the stable and metastable magnetic configurations as well as the transition states connecting them. The topology of the resulting ergodic ensemble of stationary states is analyzed from both local and energy perspectives by calculating the corresponding kinetic networks and disconnectivity graphs. For all lattices, the magnetic orders of the ground-state and low-lying metastable configurations are identified, including the elementary relaxation processes between them. A remarkable profound dependence of the collective magnetic behavior on the structural arrangement of the NPs is revealed. Square and triangular nanostructures are extremely good structure seekers, showing starlike kinetic networks and disconnectivity graphs with palm-tree form. Their continuously degenerate ground states are throughout-reaching hubs connected to nearly all excited magnetic configurations over a single first-order saddle point. Rhombic ensembles have double-funnel ELs in which the time-inversion-related ground states play the role of hubs with exceedingly high connectivity densities. These systems need to undergo very few elementary transitions with small downward energy barriers to relax from any configuration towards one of the ground states. However, the energy barriers between the two funnels are quite large and, furthermore, they increase as the number of particles in the unit cell is increased. Therefore, ergodicity breaking is expected in the thermodynamic limit. Finally, the rectangular and oblique lattices show contrasting ground-state orders, the former consists of an antiferromagnetic alternation of head-to-tail chains of spins while the latter is ferromagnetic. Nevertheless, the ELs of these nanostructures are qualitatively very similar. In both cases, all excited magnetic configurations consist of independent flipping of the chains of spins that are formed along the direction of the shorter Bravais vector. The whole energy spectrum of metastable magnetic configurations can thus be mapped to a one-dimensional Ising model. As a result, the kinetic network of stationary points is latticelike and the disconnectivity graphs have a willow-tree form. In conclusion, the collective magnetic behaviors of nanostructures having different point-group symmetries are contrasted and related by varying the parameters of the lattices that interpolate between them.

I. INTRODUCTION

Recent advances in nanoparticle (NP) synthesis, auto-organization, and structuring have made it possible to create artificial two-dimensional (2D) materials consisting of ensembles of nanoscale magnets [1–5]. These systems represent an extremely active and challenging research area from both fundamental and technological viewpoints. Indeed, finite-size effects, reduced dimensionality, and competing interactions lead to novel magnetic behaviors which are most relevant for potential applications, for example, in the fields of spintronics, memory devices, and high-density data storage [6–8]. The magnetic properties of NP ensembles are known to depend on the size and composition of the NPs, on the nature and strength of their interactions, as well as on their geometrical arrangement. Early studies of magnetism at the nanometer scale have been focused on understanding the dependence

on size, structure, and composition. Thus, remarkable enhancements of the spin moments, orbital moments, and magnetocrystalline anisotropy of small transition-metal clusters have been revealed [9–18]. Furthermore, in more recent years, the interest in the global magnetic response of NP ensembles has been growing steadily [4,5,19–24]. From this perspective, two qualitatively different regimes need to be distinguished, depending on the relative importance of single-particle local energies and interparticle coupling strengths. In weakly interacting ensembles the magnetic properties are dominated by single-particle contributions such as the NP magnetization and magnetic anisotropy. The dynamics of the ensemble is largely the result of local reorientations of the magnetic moments of individual NPs. Therefore, the details of the underlying geometry of the NP arrangement play a secondary role. A far more complex and challenging situation arises in strongly interacting ensembles, for instance, in systems consisting of closely packed, highly symmetric NPs with weak magnetocrystalline anisotropy. In this case, changes in the orientation of the magnetization of one particle inevitably

---

*gallina@uni-kassel.de

184407-1

induce changes in the magnetic order at the surrounding particles. The cooperative many-body nature of the ensemble manifests itself even in the most basic transitions between two nearby metastable magnetic configurations. Therefore, it conditions the magnetic response of the ensemble as a whole [25–27]. Under these circumstances, the structure of the ensemble of nanoparticles, the existence of translational and point-group symmetries or, in contrast, their absence due to some degree of disorder, become crucial since they define the local environment and long-range spatial correlations of the magnetic moments. The resulting physical consequences are expected to be particularly important for the dipole-coupled NPs considered in this work since this interaction is both frustrating and long range [20,24–29].

Previous investigations of the magnetic properties of two-dimensional NP ensembles have uncovered a variety of fascinating physical behaviors including long-range-order phase transitions, continuous ground-state degeneracies, and order-by-disorder effects [19,20,28–30]. In addition, remarkable nonequilibrium phenomena have been found, such as dynamical slowing down, ergodicity breaking, memory effects, and aging [31–34]. Furthermore, it has been shown how several of these effects are intrinsically related to the qualitative changes in the interaction-energy landscapes of these systems [35,36]. On the one hand, ensembles with a high point-group symmetry and a small degree of disorder are good structure seekers with a clear global energy minimum, long-range order, and fast unhindered relaxation dynamics. On the other, strongly disordered ensembles exhibit very rough and frustrated ELs with an extremely large number of low-energy local minima separated by large energy barriers, which thus leads to glasslike relaxation dynamics [35,36]. These studies demonstrate that the lattice structure in which the NPs are organized, its point-group symmetry, or the absence thereof play a central role in the equilibrium and dynamical properties of magnetic NP ensembles. Nevertheless, our understanding of the effects of lattice geometry and symmetry on the cooperative magnetic behavior of these nanostructures is still incomplete. It is the goal of this work to investigate the collective magnetic properties of NP ensembles by characterizing the energy landscapes of dipole-coupled ensembles of magnetic NPs, which are located on the regular positions of the five different 2D Bravais lattices. The distinctive features of the ELs corresponding to each periodic lattice are revealed by giving particular emphasis to analyzing how they correlate with the specific symmetries of the various NP ensembles. Aside from the fundamental theoretical interest of correlating the magnetic order and collective magnetic behavior of 2D nanostructures with the underlying structural organization of the particles, this study of periodic systems is expected to serve as a reference in order to understand the behavior of more realistic situations including, for example, structural disorder, particle-size distributions, or random local anisotropy fields.

The remainder of the paper is organized as follows. In Sec. II, the theoretical background is presented. The considered model is introduced and the various methods employed for the characterization of the ELs are illustrated. In Sec. III, the different 2D Bravais lattices are investigated and discussed in some detail by contrasting their metastable magnetic configurations, kinetic networks, and disconnectivity graphs. The paper is closed in Sec. IV with a summary of the main conclusions and by pointing out some relevant extensions and implications of this study.

II. THEORETICAL MODEL AND METHODS

The Hamiltonian of a system of classical dipole-coupled magnetic moments $\vec{\mu}_k$ located at the positions $\vec{r}_k$ reads as

$$H = \frac{\mu_0}{8\pi} \sum_{k \neq l} \left[\frac{\vec{\mu}_k \cdot \vec{\mu}_l}{r_{kl}^3} - 3 \frac{(\vec{\mu}_k \cdot \vec{r}_{kl})(\vec{\mu}_l \cdot \vec{r}_{kl})}{r_{kl}^5} \right], \quad (1)$$

where the vector $\vec{r}_{kl} = \vec{r}_k - \vec{r}_l$ connects lattice sites k and l, r_{kl} is the corresponding Euclidean distance, and μ_0 the vacuum permeability. Each magnetic moment $\vec{\mu}_k$ has a fixed modulus μ_k and its direction is characterized by the polar and azimuthal angles θ_k and φ_k. In this work, the NPs carrying the local moments are located at the regular positions of 2D Bravais lattices, whose primitive cells and point-group symmetries are illustrated in Fig. 1. In practice, the extended nanostructures are modeled by considering N particles in a unit cell with periodic boundary conditions.

A. Energy landscapes

The static and dynamic properties of a magnetic NP ensemble are governed by its underlying EL, which in the present case depends on $2N$ degrees of freedom $\{\theta_k, \varphi_k | k = 1, \ldots, N\}$. A meaningful simplification of such a complex multivariable function is to discretize it into its stationary states, namely, its local minima (LM) and first-order saddle points or transition states (TS) [37–40]. These stationary points form a connected network which, putting aside the short-time fluctuations of the magnetic configurations around the local minima, allows us to characterize the long-time stochastic dynamics of the system. The LM and TS are determined by the following algorithm, which is adapted from Ref. [41]. To get started, an initial set of metastable states is built. One or more local minima are found starting from random magnetic configurations and using the L-BFGS algorithm [42]. Subsequently, the following iterative procedure is performed: (i) Choose a LM from the database of stationary states that has not yet been used for locating new stationary states. (ii) Perform an eigenvector-following search starting along a specific eigenvector of the Hessian **H** at this LM [39,40,43]. One usually chooses the eigenvectors associated with the smallest eigenvalues of **H** since the energy increase along these directions is smallest. (iii) Once a TS is found, its two adjacent LM are identified by stepping off the TS in the directions parallel and antiparallel to the single unstable mode and, starting from there, by performing the corresponding L-BFGS minimizations [42]. (iv) If one of the two LM obtained in the previous step coincides with the initial LM, the other LM and the TS are added to the database of stationary states. (v) The algorithm proceeds by choosing a different eigenvector and repeating the steps (ii)–(iv). Once a fixed number of eigenvectors have been tried (in this work 10), the algorithm loops back to step (i) and a new LM is considered. The algorithm terminates after all LM in the database have been used as initial states.
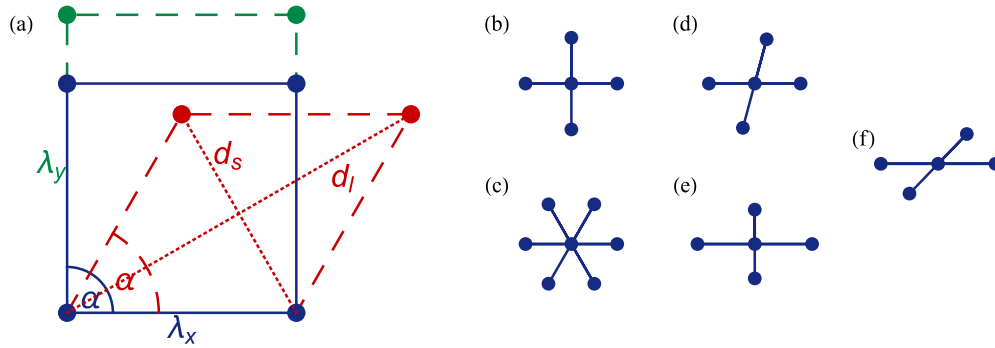
FIG. 1. Illustration of the five different types of two-dimensional Bravais lattices. In (a) the basis vectors are characterized by their lengths λ_x and λ_y and by the angle α between them. The longer and shorter diagonals d_l and d_s are also indicated here by dotted lines. For $\lambda_x = \lambda_y$ we have (b) the square lattice if $\alpha = \pi/2$, (c) the triangular lattice if $\alpha = \pi/3$, and (d) a rhombic lattice otherwise. For $\lambda_x \neq \lambda_y$ one obtains (e) a rectangular lattice if $\alpha = \pi/2$ and (f) an oblique lattice if $\alpha \neq \pi/2$.

B. Kinetic networks

The set of all LM and TS of an energy landscape forms a connected network often known as the kinetic network of the system. It can be illustrated by an undirected graph, where the LM are represented by nodes and the elementary transitions connecting two LM through an intermediate TS (first-order saddle point) are represented by an edge between them. A number of properties can be calculated in order to characterize the various kinetic networks thus allowing us to compare the topologies of the ELs in different physical situations. The *degree* $n(i)$ of node i is defined as the number of edges or TS connecting node i with any other node. As networks may vary strongly in size, i.e., in the number of nodes, it is sound to introduce the *local degree density* of node i as

$$\rho_n(i) = \frac{n(i)}{N_{\text{LM}} - 1}, \tag{2}$$

where N_{LM} is total number of LM in the network. Nodes having comparatively large values of $\rho_n(i)$ are known as *hubs*. When available, they are exceedingly important for the dynamical behavior of complex systems.

Another important network property is the *distance* d_{ij} between two nodes i and j, which is defined as the minimum number of steps or edges that are required to connect nodes i and j. The *average path distance* $\langle d \rangle$ over all pairs of nodes provides a measure of the extension of a network. Moreover, it is often meaningful to quantify the clustering in a network. A common measure of it is the *transitivity*

$$C = \frac{3 \times \text{number of triangles}}{\text{number of triads}}, \tag{3}$$

which represents the probability that in a triad of nodes ($i \neq j \neq k$), where i is connected to j and j is connected to k, also i and k are connected with each other [44].

Two simple reference models are particularly useful to compare and classify network characteristics, namely, periodic lattice structures and random networks. They have strongly contrasting properties. In a random network, the nodes are connected randomly with each other according to a given average degree [45,46]. They have relatively short average path distances $\langle d \rangle$ and small transitivities C. In contrast, in a latticelike network, all nodes have the same number of close-by neighbors. This implies large average path

distances and non-negligible transitivities, unless the network is bipartite.

A particular combination of these properties leads to the notion of small-world networks. According to Watts and Strogatz, a network can be regarded as a small world if it combines the short average-path distance of random graphs with the relatively large transitivity of lattice networks [47]. Small-world networks are further characterized by the presence of hubs having large local connectivity densities. Many naturally occurring networks are small worlds, for instance, social and neural networks. In our context, it is interesting to elucidate under what circumstances the kinetic networks of magnetic NP ensembles exhibit small-world behavior [45,46].

C. Disconnectivity graphs

Disconnectivity graphs (DGs), as proposed by Karplus *et al.*, allow us to analyze the properties of an EL from the perspective of the energies of the metastable LM and the energy barriers separating them [38]. Several examples of DGs of magnetic nanostructures are shown in Sec. III. The physical meaning of these graphs can be clarified by describing the algorithm employed to construct them (see also Refs. [38,40,48]). For any given energy E, the energetically accessible local minima, i.e., the local minima having an energy lower than E, are grouped into disjoint sets denoted as superbasins. Two LM belong to the same superbasin if there is a path, for example, the minimum energy path (MEP), which connects the two LM without ever exceeding the energy E. Usually, one starts by choosing E close to the energy of the global minimum. In the absence of degeneracies, only one superbasin, the one containing the global minimum, is accessible for such low values of E. If the ground state is N-fold degenerate, there are then N disjoint superbasins. As the energy E is gradually increased, more local minima are found with energies lower than E. However, in most cases, these newly found LM cannot be connected to the ground state without exceeding the energy E. Therefore, one usually observes that the number of superbasins first increases. Nevertheless, at some point, the superbasins start to merge with each other since the separating energy barriers along the connecting MEP can be overcome. Eventually, for very high values of E, only one superbasin is left, which contains all local minima of the system, provided that the energy barriers are finite.

In practice, the DGs are obtained by performing the above-described analysis at a discrete set of equidistant energies, which are sometimes indicated on the y axis. At each energy E, a superbasin is represented by a vertical segment. Two segments are connected with each other, if they share at least one local minimum. The position of these along the horizontal x axis is arbitrary. It is usually chosen in a way that superbasins separated by lower-energy barriers are closer to each other than those separated by larger energy barriers. In the end, the result is a treelike graph, where the end point of each branch gives the energy of the corresponding local minimum and the merging point of two branches indicates the energy barrier which separates them. See, for instance, the DGs shown in Sec. III or in Refs. [35,36].

III. RESULTS

The goal of this section is to determine the magnetic properties of dipole-coupled NPs organized in 2D periodic arrangements having different lattice symmetries by exploring the interaction-energy landscapes of these nanostructures. For this purpose, we consider all the different Bravais lattices which can be constructed in two dimensions: square, triangular, rectangular, rhombic, and oblique lattices. Aside from the fundamental interest of characterizing the properties of the idealized periodic arrangements, the present investigations are also important as a reference in view of assessing and understanding the consequences of disorder inherent to experimental samples [35].

The extended nanostructures are modeled with finite unit cells having $N = 36$ magnetic dipoles and periodic boundary conditions. In order for the energies to be comparable, the surface coverage, i.e., the surface per particle, is the same in all cases. Moreover, the energies are measured in units of the interaction energy of a pair of parallel nearest-neighbor (NN) magnetic moments pointing perpendicular to the vector connecting them, which is given by

$$\varepsilon_{DD} = \frac{\mu_0}{8\pi} \frac{\mu^2}{r_0^3}, \tag{4}$$

where r_0 is the NN distance. For example, in a system composed of Fe particles with a diameter $\phi = 3$ nm and $\mu \simeq 2.6 \times 10^3 \mu_B$ at a distance $r_0 = 5$ nm one has $\varepsilon_{DD} = 1.4$ meV [35].

A. Square lattice

The periodic square lattice is defined by $\lambda_x = \lambda_y$ and $\alpha = \pi/2$ (see Fig. 1). Its point-group symmetry with respect to a lattice site is the direct product of the group D_4 and the inversion group $\{E, I\}$. It contains 16 symmetry operations. First, we have the $\pi/2$ rotations E, C_4, C_4^2, and C_4^3 around the axis perpendicular to the lattice plane and the four π rotations U_2 around the axes passing through the middle of opposite sides or along the diagonals of the squares, which comprise the group D_4. The remaining symmetries are the four reflections across the vertical planes defined by the U_2 in-plane axes and the vertical C_4 axis, the inversion I, the

reflection σ_h across the horizontal plane of the lattice, and the two rotoreflections $C_4\sigma_h$ and $C_4^3\sigma_h$.

In Fig. 2, representative magnetic configurations of the ground state and of the first and second metastable states are shown for a periodic square lattice with $N = 36$ magnetic NPs in the unit cell. The ground-state magnetic configurations are known to be microvortex (MV) states, where the orientations of the magnetic moments $\vec{\mu}_k$ at each lattice site k are given by

$$\vec{\mu}_k = \begin{bmatrix} \mu_k^x \\ \mu_k^y \end{bmatrix} = \begin{bmatrix} (-1)^{n_y}\mu \, \cos(\eta_{MV}) \\ (-1)^{n_x}\mu \, \sin(\eta_{MV}) \end{bmatrix}, \tag{5}$$

where $\eta_{MV} \in [0, 2\pi]$ is the microvortex angle, n_x and $n_y \in \mathbb{Z}$ indicate the position of site k along the x and y directions of the square lattice, and $\mu = |\vec{\mu}_k|$ is the modulus of the magnetic moments [19,28,30]. For instance, $\eta_{MV} = 0$ corresponds to the striped antiferromagnetic state shown in Fig. 2(a) and $\eta_{MV} = \pi/4$ corresponds to a perfect vortex state shown in Fig. 2(b). In the absence of lattice distortions, the MV state is continuously degenerate with respect to η_{MV}. This can be shown to be a consequence of the quadratic form of the dipole-dipole interaction energy and the C_4 rotational symmetry of the square lattice [28,30]. The continuous ground-state degeneracy of the MV state can be broken by thermal fluctuations because the curvature of the energy landscape is different for different values of η_{MV}. It is also known to be broken by structural disorder and distortions. The resulting stabilization of a few states out of a continuous set of degenerate ground states is known as the order-by-disorder effect [49–51].

In contrast to the ground state, the degeneracies of the excited states are finite. They are a consequence of the point-group and translational symmetries of the lattice. In Figs. 2(c) and 2(d) one observes that in the lowest excited configurations the magnetic moments arrange primarily in microvortices, where the local magnetic moments $\vec{\mu}_k$ do not align along the x and y axes defined by the Bravais vectors but rather along the diagonals (i.e., $\varphi = \pm\pi/4$ or $\pm 3\pi/4$). The first excited configuration can be obtained from the ground state having $\eta_V = \pi/4$ by interchanging two vertical and two horizontal neighboring lines of magnetic moments with each other. Consequently, the net magnetization is zero as in the ground state. The periodicity of the configuration with respect to translations along the x and y axes, which in the $\eta_{MV} = \pi/4$ ground state was two lattice spacings, is now completely removed within the unit cell. The absence of any intrinsic translational invariance implies that all 36 translations within the unit cell yield different degenerate configurations. Moreover, due to the time-reversal symmetry of the Hamiltonian, the energy remains unchanged upon inverting locally all magnetic moments (i.e., $\vec{\mu}_k \to -\vec{\mu}_k$). Since an inversion changes the sense of the vortices (see Fig. 2) 36 new degenerate configurations are obtained. This raises the total degeneracy of the first excited state to 72. The symmetry operations of the D_4 group do not yield any additional degenerate magnetic configurations in this case since they result in states identical to some translation [see Fig. 2(c)].

The second excited state is obtained from the ground state having $\eta_{MV} = \pi/4$ by interchanging the spin orientations of two horizontal and two vertical lines of magnetic moments
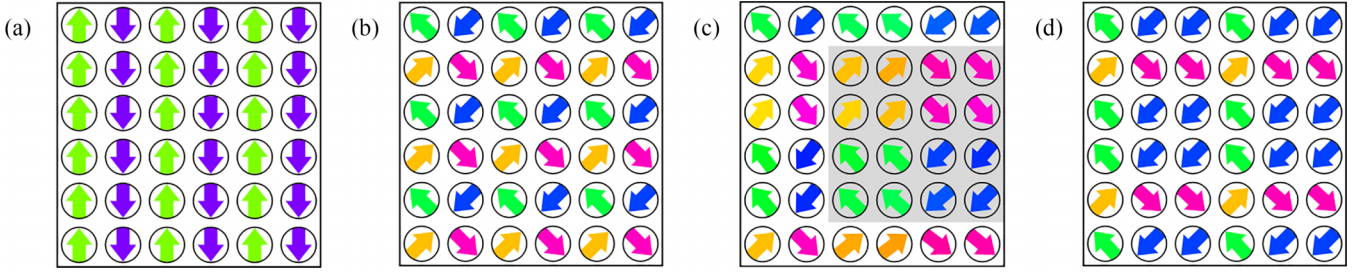
FIG. 2. Lowest-energy metastable magnetic configurations of a periodic square lattice with $N = 36$ dipole-coupled NPs in the unit cell. The circles indicate the position of the particles while the arrows indicate the orientation of the magnetic moments within the xy plane. Examples of the configurations of the continuously degenerate ground state are shown in (a) for $\eta_{\mathrm{MV}} = 0$ and (b) for $\eta_{\mathrm{MV}} = \pi/4$ [see Eq. (5)]. The configurations of the first and second excited states are shown in (c) and (d), respectively.

as in the first excited state, and by rotating in addition the magnetic moments on one of the horizontal and one of the vertical interchanged lines by π. In contrast to the ground state and the first excitation, the second excited state has a finite in-plane net magnetization. The periodicity of this configuration with respect to translations along the x and y directions is three lattice spacings. As a result, nine different degenerate configurations are obtained. For each of these, the four elements of the C_4 group yield different states since they have different in-plane magnetizations. This explains the 36-fold degeneracy of the second excited state. Time inversion does not yield any new states since the time-inverted configurations can also be obtained through a π rotation followed by an appropriate translation. Notice that for this to be possible it is necessary that the average rotation of the magnetic configuration vanishes. Further excited states could not be found for the considered unit-cell size having $N = 36$ particles.

The energy landscapes of ensembles of dipole-coupled magnetic moments usually contain a large number of local minima, which are connected through diverse transition states [25–27,35,36]. Each LM-TS-LM triplet represents an elementary transition or relaxation process, the combination of which determines the stochastic dynamics of the system. In the present case, as a consequence of the high symmetry of the square lattice, we find only $N_{\mathrm{LM}} = 109$ local minima, assuming that the degenerate ground state is counted as one, and $N_{\mathrm{TS}} = 288$ first-order transition states connecting them. A first insight into the topology of the EL of the square lattice is provided by the kinetic network shown in Fig. 3(a). Here, the nodes represent the LM and the edges the connecting TS, thus demonstrating the connectivity among the LM. Remarkably, the ground state (red node) is directly connected to all the excited states, while there are no direct LM-TS-LM connections at all between any pair of excited states. Hence, the degree density of the ground state is $\rho_n = 1$, i.e., it is a throughout-reaching hub. One concludes that the basin of attraction of the ground state is extremely large. This is a consequence of its continuous degeneracy, which allows the system to always adapt its lowest-energy configuration to the most suitable one in order to reach all the different excited states over a single energy barrier. The resulting network, denoted as a star S_{108} in graph theory, has some fascinating properties [52]. For once, the distance between any pair of excited states is $d = 2$ elementary transitions, while the distance between any excited

state and the ground state is $d = 1$. This results in a average path distance $\langle d \rangle = 1.99$. Moreover, a star network is bipartite since there are no loops, the continuous ground state building one sublattice and the 108 excited states the other. Hence, the transitivity of a star network is $C = 0$.

From a physical perspective, the starlike topology of the kinetic network (KN) is the most clear sign of a very fast relaxation from any excited state towards the ground state since the latter is at the center of the network and only one energy barrier has to be overcome. Furthermore, the dynamics is completely funneled because there are no connections between the excited states. One concludes that the square-lattice NP arrangement is an extremely good structure seeker [53]. As expected, the periodic arrangement shares many of its characteristics with slightly disordered square-lattice ensembles [35,36]. However, it may be interesting to note that the kinetic network of periodic square-lattice ensembles shown in Fig. 3(a) does not strictly match the usual definition of small world behavior, in contrast to the slightly disordered counterpart, despite the fact that the $\langle d \rangle$ is so small [35,36]. The reason for this is the vanishing transitivity. Nevertheless, the fact that $C = 0$ is not expected to have any significant impact on the unhindered relaxation dynamics of the system.

While the kinetic network reflects the connectivity of the metastable states, it provides no insight on the energies involved in the elementary transitions. A most needed complementary characterization of the energy landscape is provided by the disconnectivity graphs. Here, the focus no longer resides on the connectivity among the metastable states but on their energies and on the energy barriers separating them. In Fig. 3(b) the DG of the periodic square-lattice ensemble illustrated in Fig. 2 is shown. In order to improve its readability, degenerate states have been grouped by representing them with a single branch. The energy barriers from any of these configurations towards the ground state are the same. The number of degenerate metastable states belonging to each branch is indicated.

The continuously degenerate ground state is easily recognizable at the bottom of the disconnectivity graph, with all excited states located at much larger energies. Notice that the energy profiles are extremely asymmetric, as the energy barriers from any excited state towards the ground state are very small, while the energy barriers from the ground state to any excited state are about 10^2–10^4 times larger. Therefore, starting from any given initial state, the system
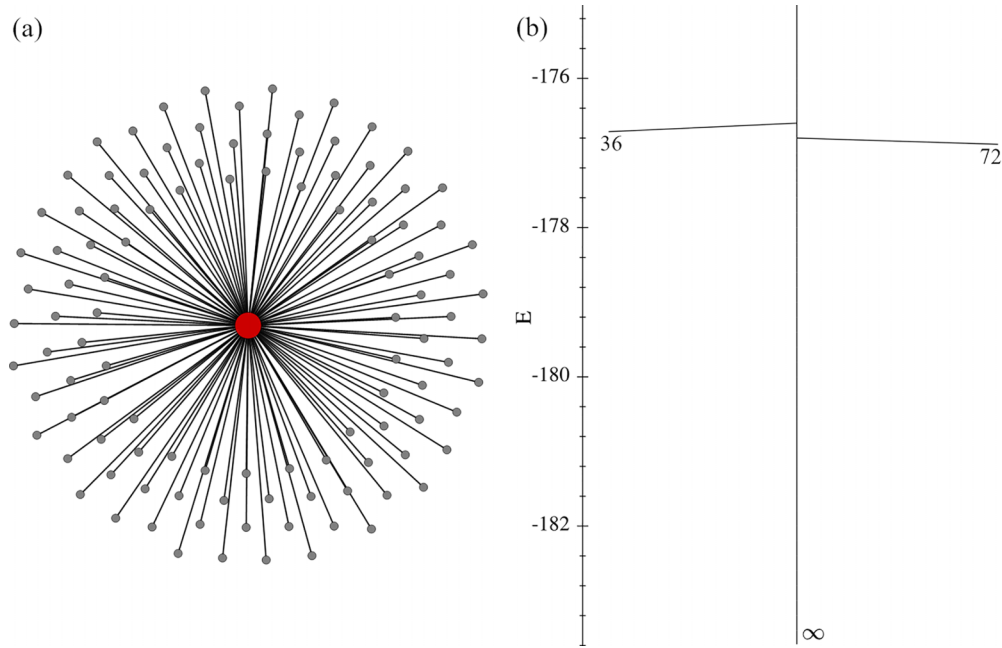
FIG. 3. (a) Kinetic network of local minima (nodes) and transition states (edges) and (b) disconnectivity graph of the energy landscape of a periodic square lattice with $N = 36$ dipole-coupled NPs in the unit cell. In (b) degenerate states are grouped together and the degeneracy is indicated at the corresponding branch. Energies are given in units of ε_{DD} [Eq. (4)]. The ground state shows a continuous degeneracy with respect to the microvortex angle. See also Fig. 2 and Eq. (5).

relaxes most rapidly and irreversibly towards the ground state, even at relatively low temperatures. The analysis of the DG complements the information provided by the kinetic network and is in qualitative agreement with the behavior found for weakly disordered square-lattice ensembles [35,36].

The ELs of two-dimensional square-lattice arrangements of magnetic moments have been previously investigated in the framework of the classical XY model [54,55]. Despite the common focus on the collective behavior of interacting local magnetic degrees of freedom, there are profound differences in the physics behind the XY model and the present description of ensembles of magnetic nanoparticles. The latter concerns spins interacting through NN ferromagnetic couplings and therefore lacks long-range and competing effects. Furthermore, the intrinsic continuous 2D spin-rotational symmetry is artificially removed in the calculations by keeping one spin fixed [54,55]. This contrasts with the present NP ensembles which are subject to dipolar magnetic couplings which are anisotropic, long ranged, and frustrated. Nevertheless, it is interesting to observe that the EL of the XY model corresponds to an efficient relaxation towards the global minimum, i.e., to a good structure seeker. This behavior is qualitatively similar to what we observe in the periodic square lattice, as well as in previous studies of weakly disordered NP ensembles [35,36]. Moreover, the downhill energy barriers separating the metastable minima and the lower-lying spin arrangements are in both cases very small. It would be interesting to extend the investigations on spin models by characterizing the ELs corresponding to other lattice structures and magnetic couplings, particularly when competing interactions and magnetic frustrations are present.

B. Triangular lattice

The triangular lattice is defined by $\lambda_x = \lambda_y$ and $\alpha = \pi/3$ and its point-group symmetry is the direct product of D_6 and the inversion group $\{E, I\}$. It consists of 24 operations (see Fig. 1). First we have the D_6 group: the six $\pi/3$ rotations around the principal C_6 axis perpendicular to the lattice plane and the six π rotations U_2 around the axis passing either along a nearest-neighbor bond or through the middle of the bonds between nearest neighbors. Combining them with the inversion group gives the inversion I, the reflection across the horizontal plane σ_h, four rotoreflections of the form $S_6 = C_6^n \sigma_h$ with $n = 1, 2, 4$ and 5, and the reflections across the six vertical planes defined by the U_2 axes and the principal C_6 axis.

In Fig. 4 the ground-state magnetic configuration (a), the first excited state (b), and the second excited state (c) are shown. The ground state is known to be ferromagnetic and continuously degenerate with respect to the orientation of the magnetic moments [29,35]. This is a consequence of the D_6 point-group symmetry of the triangular lattice. As in the square lattice, this continuous degeneracy is lifted by thermal fluctuations, structural disorder, or distortions [35]. The first and second metastable states are low-symmetry vortexlike magnetic textures, in which the orientations of all local moments change with respect to the ground state. These configurations have a small or vanishing average magnetization per particle ($m = 0.15\,\mu$ and $m = 0$ for the first and second excited states, respectively) which strongly contrasts with saturated ground state ($m = \mu$). The first excited state shows no periodicity within the unit cell. Thus, translations yield a 36-fold degeneracy. Furthermore, since the average magnetization is finite all elements of the C_6 group yield
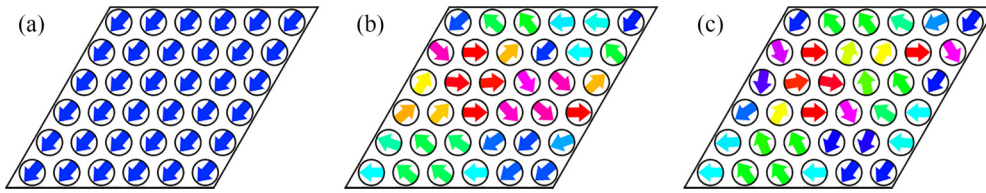
FIG. 4. Lowest-energy magnetic configurations of dipole-coupled NPs on a periodic triangular lattice with $N = 36$ particles in the unit cell. The circles indicate the position of the particles while the arrows indicate the orientation of the magnetic moments within the xy plane. One of the magnetic configurations of the degenerate ground state (a), first excited state (b), and second excited state (c) are shown.

different configurations, which brings the degeneracy to 216. Finally, since the average rotation of the magnetization field is finite [see Fig. 4(b)], it follows that time inversion enhances the degeneracy by an additional factor 2. This accounts for the observed 432-fold degeneracy of the first metastable state.

In the case of the second metastable state, the degeneracy due to translations is also 36. However, in this case, only a $\pi/3$ rotation around the principal C_6 axis results in different magnetic configurations. Further rotations around the C_6 axis yield states that can be obtained through a translation, a $\pi/3$ rotation, or a combination of both. Notice that such an intrinsic invariance is possible only when the average magnetization vanishes. Finally, as in the first excited configuration, the average rotation of the magnetization field is finite. Therefore, time inversion leads to new states, which raises the degeneracy of the second excited state to 144. Two further metastable states are found at comparable or somewhat higher energies, the symmetry of which is very low, as in the first excited state. Analogous considerations show that the degeneracies of these states are also equal to 432.

In order to investigate the connectivity and elementary transitions among the metastable states of the triangular-lattice system, we have determined the corresponding kinetic network, which is shown in Fig. 5(a). The network consists of $N_{LM} = 1650$ local minima (represented by the nodes) and $N_{TS} = 5280$ transition states (represented by the edges). One observes that the continuously degenerate ground state, highlighted by the red circle, is at the center of the network. Most of the excited states are directly connected to it. However, in contrast to the square lattice [Fig. 3(a)] one finds here direct connections between pairs of excited states, i.e., first-order saddle points allowing for elementary transitions between metastable configurations. Hence, the kinetic network of the triangular lattice is not strictly bipartite. Still, most of the excited states are directly connected to the ground state, which thus represents a hub with nearly maximum degree density $\rho_n = 0.91$. Consequently, the average path distance $\langle d \rangle = 2.17$ is remarkably small for a network of this size. In addition, the transitivity $C \approx 10^{-3}$ is extremely small. One concludes that the kinetic network of the triangular lattice is very close to starlike. Therefore, the topography of the EL remains qualitatively similar to what is observed for the square lattice.

From a physical perspective, the results show that the relaxation dynamics of dipole-coupled NPs forming a triangular lattice should be extremely fast since the vast majority of the excited states are directly connected to the ground state. In this regard, the kinetic networks of square and triangular en-

sembles share their main characteristics of very good structure seekers. It has been shown that weakly disordered triangular lattices also have this property [35]. Although the average distance $\langle d \rangle = 2.17$ between the LM is very small, one cannot say that the KN of the perfect triangular lattice matches the typical small-world behavior since the transitivity $C \approx 10^{-3}$ is very small. This contrasts with the properties found when a weak degree of disorder in the NP positions is taken into account. In fact, weak disorder lifts the degeneracies among the LM and multiplies the possibilities for elementary transitions among them. Thus, the transitivity is raised in a most significant way without significantly increasing $\langle d \rangle$ [35].

The disconnectivity graph of the triangular lattice with $N = 36$ particles in the unit cell is shown in Fig. 3(b). As before, degenerate states are grouped, representing them by a single branch, provided that the energy barriers towards all other states are identical. The ground state is easily recognizable at the bottom of the DG, clearly separated from all the excited states which are located at much larger energies. This leads to a very asymmetric energy profile, as in the case of the square lattice. The downhill energy barriers towards the ground state are extremely small, while the energy barriers in the opposite uphill direction are quite large. As a consequence, the system relaxes most rapidly and irreversibly from any excited state towards the ground state. This behavior is consistent with the previously discussed properties of the KN. One concludes that periodic triangular-lattice ensembles of magnetic NPs are indeed remarkably good structure seekers, as the periodic square-lattice ensemble or the previously studied weakly disordered ensembles [35].

C. Rectangular lattice

A rectangular lattice is characterized by $\lambda_x \neq \lambda_y$ and $\alpha = \pi/2$. It has a D_2 point-group symmetry, as well as the general time-inversion symmetry. One does not expect any continuous metastable state degeneracies as, for instance, in periodic square or triangular lattices, since the two-dimensional representation (x, y) which is irreducible with the groups C_4 and C_6 is now reducible. To be specific, we focus the following discussion on a rectangular lattice having $\lambda_x/\lambda_y = 1.05$. The results, however, are also representative of ensembles with larger λ_x/λ_y. In fact, our calculations show that larger λ_x/λ_y ratios do not lead to qualitative differences in the physical behavior but only to a quantitative enhancement of the consequences of breaking the symmetry of the square lattice. The trends found in the transition regime, close to the square-lattice arrangement $(1 < \lambda_x/\lambda_y < 1.05)$, are pointed out at the end of this section.
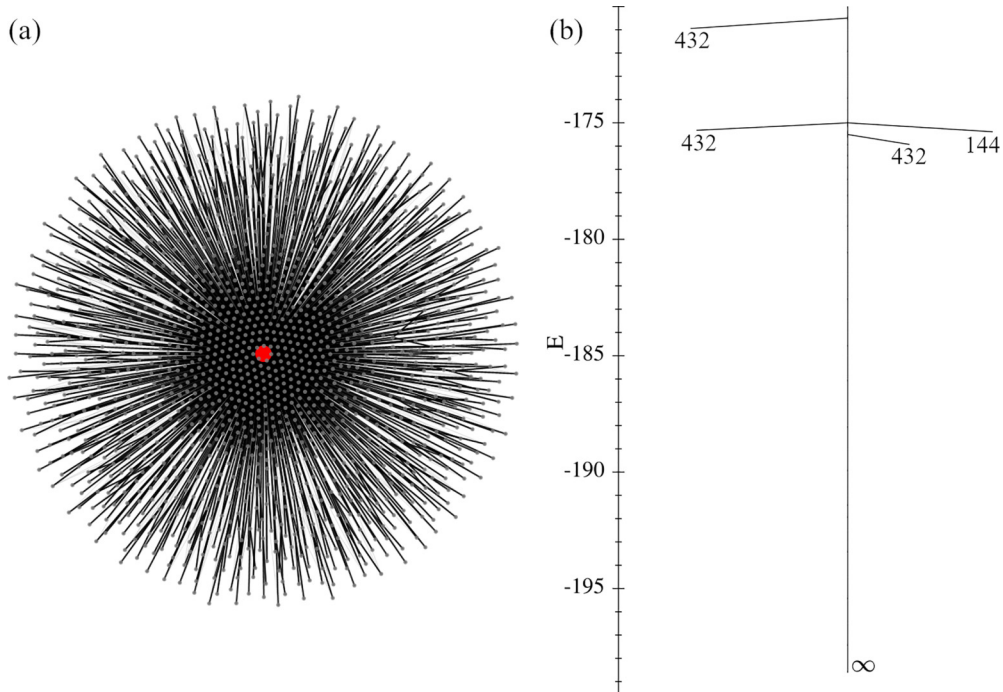
FIG. 5. (a) Kinetic network of local minima (nodes) and transition states (edges) and (b) disconnectivity graph of the energy landscape of a periodic triangular lattice with $N = 36$ dipole-coupled magnetic moments. In (b) the degenerate states are grouped together and the degeneracy is indicated at the corresponding branch. The ferromagnetic ground state shows a continuous degeneracy with respect to the angle defining the direction of the magnetization (see also Fig. 4).

In Fig. 6 the magnetic configurations of the ground state and the three lowest metastable states are shown ($N = 36$ and $\lambda_x/\lambda_y = 1.05$). One observes that the magnetic moments form head-to-tail spin chains along the direction y with the shorter NN distance. The ground-state configuration [Fig. 6(a)] consists of an antiparallel arrangement of these chains whose orientation alternates as we move along the x direction. The continuous degeneracy of the square arrangement is broken since $\lambda_x \neq \lambda_y$ yet the ground state belongs to the continuous manifold of MV configurations defining the ground state of periodic square lattices (Sec. III A). Out of the continuous MV manifold, only the antiferromagnetic state with head-to-tail chains along the direction with the shortest interparticle distance remains stable. The degeneracy of the ground state is thus twofold since the magnetic configuration is invariant upon translations along y and time inversion is equivalent to a translation along x [see Fig. 6(a)].

The following lowest-lying metastable LM can be obtained from the ground state by reversing the orientation of two neighboring chains of magnetic moments [cf. Figs. 6(a) and 6(b)]. This state has also a vanishing net magnetization but is not directly connected to the ground state through a single LM-TS-LM elementary transition. Translations of the first metastable state along the x axis yield six different degenerate configurations, whereas translations along the y direction do not yield any new states [see Fig. 6(b)]. In addition, time inversion enhances the degeneracy by a factor of 2, resulting in a 12-fold degeneracy for the first excited state.

The second excited state can be obtained from the first one by reversing the magnetic moments of one additional chain of spins, thus resulting in a nonvanishing net magnetization [cf. Figs. 6(b) and 6(c)]. The periodicity of this state with respect to translations along x is three lattice spacings. Together with time inversion, this yields a total degeneracy of
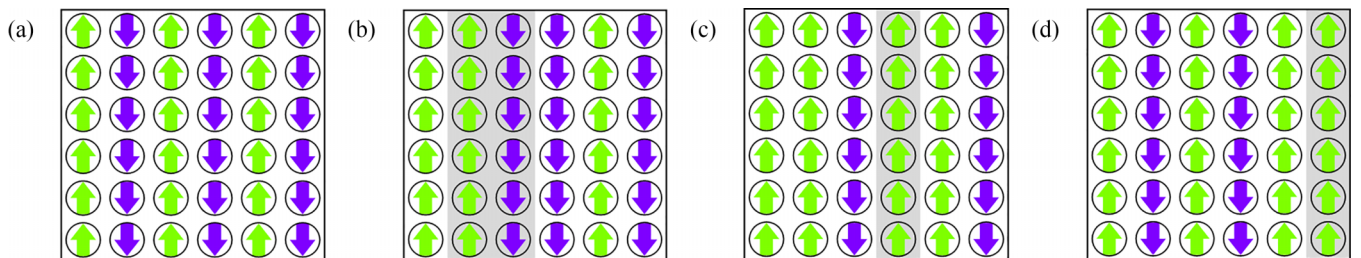

FIG. 6. Magnetic configurations of (a) the ground state, (b) the first excited state, (c) the second excited state, and (d) the third excited state of a rectangular ensemble having $N = 36$ magnetic moments in the unit cell with periodic boundary conditions. The ratio between the longer and shorter NN distances is $\lambda_x/\lambda_y = 1.05$ (see Fig. 1).
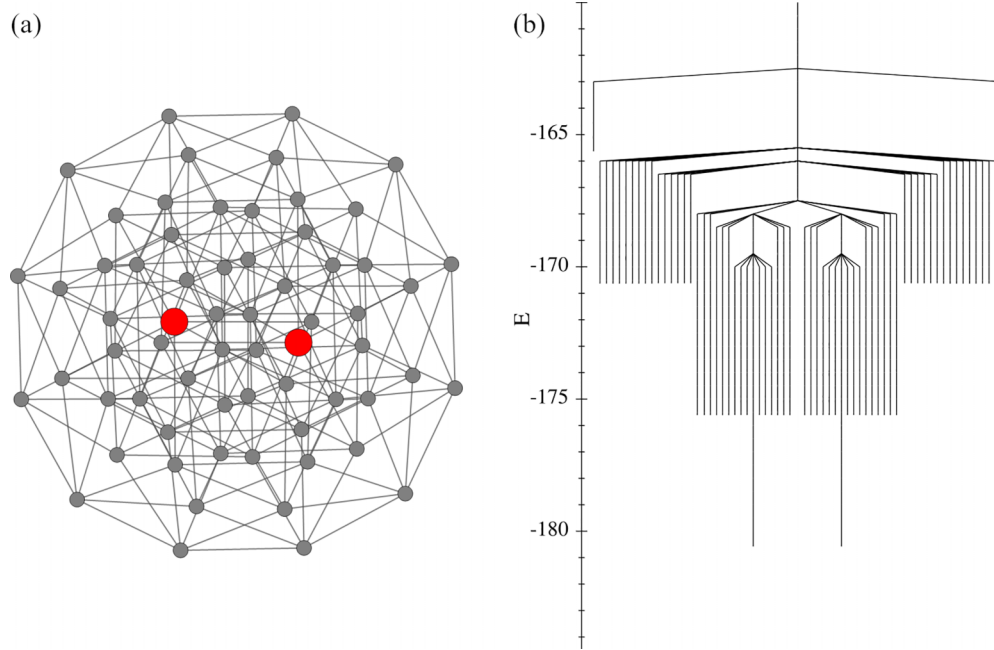
FIG. 7. (a) Kinetic network of local minima (nodes) and transition states (edges) and (b) disconnectivity graph of the energy landscape of a periodic rectangular arrangement of magnetic NPs with $\lambda_x/\lambda_y = 1.05$, $N = 36$ dipole-coupled magnetic moments in the unit cell and periodic boundary conditions (see also Fig. 6).

six for the second excited state. It is interesting to note that all other metastable states can be obtained in a similar way, by flipping the magnetic moments of spin chains along y. For example, the third excited state consists of reversing one chain of spins in the antiferromagnetic ground state and is 12-fold degenerate. In fact, the total number of local minima N_{LM} in all investigated rectangular lattices with $\lambda_x/\lambda_y \geqslant 1.05$ is 2^L, which corresponds to the number of distinct configurations that one may construct with L chains of spins along the direction with the shorter NN distance. In the present calculation, we have $L = 6$ and thus $N_{\mathrm{LM}} = 2^L = 64$. One concludes that the spin chains behave like Ising spins pointing either along $(0,1,0)$ or $(0,-1,0)$.

A detailed picture of the properties of rectangular dipole-coupled systems is provided by the kinetic network and disconnectivity graph shown in Fig. 7. The $N_{\mathrm{LM}} = 64$ local minima or nodes of the kinetic network are connected through $N_{\mathrm{TS}} = 384$ transition states or edges. Comparisons with the square and triangular lattices reveal remarkable differences (see also Figs. 3 and 5). In the rectangular arrangement ($\lambda_x/\lambda_y \geqslant 1.05$) the elementary transitions or edges are evenly distributed among the LM or nodes of the network. Indeed, each LM is connected to precisely $L = 6$ other LM, which are those obtained from the initial one by reversing one of the L chains in the unit cell (see Fig. 6). One therefore expects to find at least as many transition states as the number of these pairs, namely, $N_{\mathrm{LM}}L/2 = 2^L L/2 = 192$. It turns out that for each pair of LM differing by just one reversed chain of local moments there are two different MEPs connecting them: one in which the magnetic moments are rotated coherently clockwise within the xy plane and the other in which the rotation is counterclockwise. This explains the total number of transition states $N_{\mathrm{TS}} = N_{\mathrm{LM}}L = 384$. The transition rates

of different elementary transitions between the same pair of LM can be summed up. Hence, the KN can be simplified by representing them with a single edge. It is worth noting that no direct elementary transition, one connecting two LM through a single TS, has been found between LM that differs by more than one reversed chain of spins. Transitions between LM differing by more than one flipped chain are of course possible since the KN is ergodic. They involve a succession of single-chain flips.

The rectangular system for $\lambda_x/\lambda_y \geqslant 1.05$ can be regarded as a 1D ring of Ising spins. The correlated nature of elementary transitions is extremely strong along the short-distance direction and essentially absent in the perpendicular long-distance one. Thus, the relaxation dynamics can be pictured as the succession of individual, largely uncorrelated flips of chains of spins. This implies that the KN is bipartite with a transitivity $C = 0$ since only even loops are possible. Clearly, there are no hubs although the degree of each node grows linearly with system size. In fact, the degree density $\rho_n = L/2^L$, which is the same for all LM, vanishes exponentially as the size L of the unit cell increases. Such a periodic latticelike KN does not result in fast relaxation dynamics because many elementary transitions are required to relax and achieve equilibrium throughout the EL [45,46]. These trends are consistent with the comparatively large values of the average distance $\langle d \rangle = \sum_{i=1}^{L} i \binom{L}{i}/(2^L - 1)$, which are larger than those of a random network having the same number of nodes and edges. For instance, in the present case we have $\langle d \rangle = 3.0$ whereas the corresponding random network has $\langle d \rangle_R = 2.5$. Consequently, from the perspective of kinetic networks, one concludes that rectangular systems are not good structure seekers, in contrast to the square and triangular systems [35,56].

The KN of rectangular magnetic NP arrangements having $\lambda_x/\lambda_y \geqslant 1.05$ are qualitatively different from typical small-world networks, in particular, due to the absence of hubs and the vanishing transitivity. Nevertheless, it is interesting to note that the average distance between the nodes grows relatively slowly with the number of local minima, namely, as $\langle d \rangle \sim \ln N_{\mathrm{LM}}$. This is not very different, though still somewhat slower than the results found in small-world networks: typically $\langle d \rangle \sim \ln N_{\mathrm{LM}}/\ln\langle n \rangle$, where $\langle n \rangle$ is the average degree. That $\langle d \rangle \sim \ln N_{\mathrm{LM}}$ in the rectangular arrangement is quite remarkable for a latticelike network. The reason behind such a slowly growing $\langle d \rangle$ in relation to N_{LM} is the linear increase of the degree $n = L$ with increasing lateral dimensions.

The corresponding DG is shown in Fig. 7(b). One observes that not only the ground state but also the excited states are remarkably stable locally. In fact, all LM are separated by energy barriers which are significantly larger than the energy differences between the connected states. Moreover, there is a clear hierarchy among the energies of the ground state and the various groups of excited states. Notice, for example, that the first, second, and third metastable configurations (altogether 30 LM) have almost exactly the same energy since they all involve two frustrated NN chains of parallel spins [see Figs. 6(b)–6(d)]. Thus, the DG of the rectangular resemble corresponds closely to the so-called willow-tree type [57]. Complex systems having this type of energy-landscape topology are expected to exhibit a funneled relaxation towards their ground states as in good structure seekers, although only on a potentially much longer timescale or at relatively high temperatures [57,58]. Indeed, once $k_B T$ is of the order of the energy barrier involved in reversing one chain of head-to-tail magnetic moments, the relaxation dynamics follows in an unhindered way. The same holds even at lower temperatures on the corresponding longer inverse rate for such an elementary transition. This behavior has been observed, for instance, in C_{60} fullerenes [57,59,60]. Numerical simulations have shown that these systems relax towards their ground states at a significant rate, provided that the temperature is large enough to allow overcoming the energy barriers [57,58]. However, one should keep in mind that in rectangular NP ensembles the average number of elementary transitions required to relax towards the ground states, or to the statistical equilibrium distribution, increases strongly with the system size N. Hence, the situation is probably not as clear-cut as in C_{60}. Further investigations including explicit simulations of the relaxation dynamics, as well as a size scaling analysis, would be necessary to clarify their dynamical behavior.

In order to pursue our analysis of rectangular NP lattices, it is useful to associate an Ising spin S_i to each chain of magnetic moments along the y direction, which corresponds to the shorter NN distance λ_y. The interaction between the chains can be approximated by the spin Hamiltonian

$$E = J \sum_i S_i S_{i+1}, \qquad (6)$$

where $J > 0$ is the coupling between adjacent chains and $S_i = \pm 1$ is the Ising spin describing the ith chain along the perpendicular x direction. Taking into account that in the present case $i = 1$–6, the model predicts two degenerated ground states with energy $E_0 = -6J$, 30 first excited states

with energy $E_1 = -2J$, 30 second excited states with energy $E_2 = 2J$, and two third excited states with energy $E_3 = 6J$. Comparison with the disconnectivity graph of Fig. 7(b) shows that the model reproduces remarkably well the energy differences between the different groups of local minima by setting $J \simeq 1.25\,\varepsilon_{DD}$. One concludes that the energy spectrum of the metastable states in rectangular-lattice ensembles is indeed quite accurately captured by a simple Ising model. Although some of the degeneracies predicted by Eq. (6) are lifted by the dipolar stray fields, these energy differences are always much smaller than J for $\lambda_x/\lambda_y \geqslant 1.05$.

The Ising model also allows us to understand qualitatively how the EL changes as a function of λ_x/λ_y. In general, the coupling J between neighboring chains weakens as λ_x/λ_y increases since dipole-dipole interactions between the chains decreases as the distance between them increases. The reduction of J causes the energy differences between the local minima of the actual EL to decrease since they are primarily given by this coupling. In the limit $\lambda_x/\lambda_y \gg 1$, the individual chains along the y axis behave nearly independently from each other and all local minima have almost the same energies. In practice, this limit is nearly reached already for $\lambda_x/\lambda_y \simeq 1.4$.

Rectangular systems with ratios closer to unity ($\lambda_x/\lambda_y < 1.05$) have also been studied. Their behavior cannot be shaped into a simple model as in the case of larger ratios since the characteristic features of the square lattice become increasingly noticeable as λ_x/λ_y approaches 1. On symmetry grounds it is clear that the slightest deviation from $\lambda_x/\lambda_y = 1$ is sufficient to lift the continuous C_4-inherited degeneracy of the ground state of the square lattice and to stabilize the twofold degenerate antiferromagnetic state shown in Fig. 6. However, for $\lambda_x/\lambda_y \simeq 1$ one observes that the ELs are qualitatively very different from those found for $\lambda_x/\lambda_y \geqslant 1.05$. For $\lambda_x/\lambda_y \simeq 1$ most of the above-discussed magnetic configurations (Fig. 6) are unstable. Furthermore, the energy barriers between the two ground states, or between the excited states and the ground states, are significantly smaller. The correlations between the spin chains become important and the excitations can no longer be described by an Ising-type model. Overall, as λ_x/λ_y approaches unity, the general behavior of rectangular lattices is found to resemble the one observed in weakly disordered square lattices [35,36].

D. Rhombic lattice

The periodic rhombic lattices, also denoted as centered rectangular lattices, are defined by $\lambda_x = \lambda_y$ and $\pi/3 < \alpha < \pi/2$ (see Fig. 1). Since $\alpha = \pi/3$ corresponds to the triangular lattice and $\alpha = \pi/2$ to the square lattice, varying α allows us to interpolate between these two contrasting limits, where the behavior naturally tends to the one observed for the corresponding higher-symmetry arrangements. However, with increasing deviations of α from these extremes, the properties of rhombic ensembles change qualitatively and become very different from those of the triangular and square lattices. All rhombic ensembles have a D_2 point-group symmetry and the usual time-inversion symmetry. Consequently, as the rectangular lattice, the continuous degeneracies found in higher-symmetry square and triangular lattices are not present. In order to discuss the specific energy landscapes of
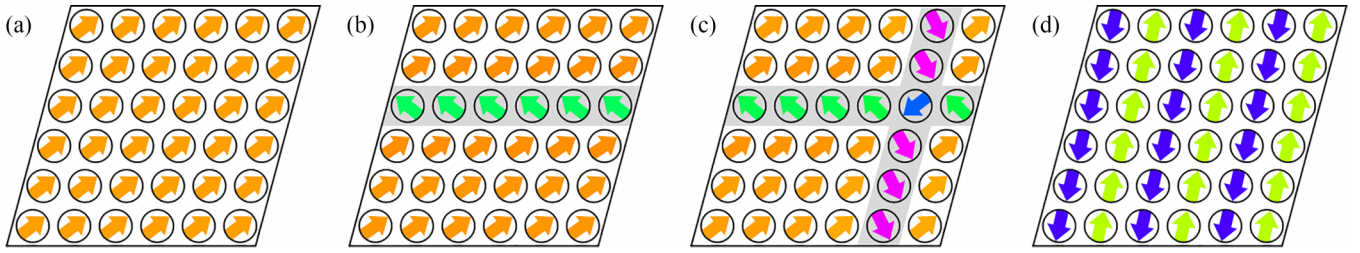
FIG. 8. Magnetic configurations of (a) the ground state, (b) the first excited state, (c) the second excited state, and (d) a higher-energy antiferromagnetic configuration of the rhombic ensemble having $\alpha = 5\pi/12$ and $N = 36$ NPs in the unit cell (see Fig. 1).

rhombic NP arrangements, we focus in the following on an ensemble having $\alpha = 5\pi/12$, which is the midpoint of the $[\pi/3, \pi/2]$ interval.

Figure 8 shows magnetic configurations of (a) the ground state, (b) the first excited state, (c) the second excited state, and (d) a particularly interesting higher excited state of a rhombic-lattice ensemble having $\alpha = 5\pi/12$, $N = 36$ magnetic NPs in the unit cell, and periodic boundary conditions. The ground state is ferromagnetic with the magnetic moments aligned along the long diagonal of the rhombic lattice. This corresponds to the ferromagnetic configuration having the smallest energy curvature in the continuously degenerate ground state of the triangular lattice. In other words, at this point changes in the relative orientation of the magnetic moments cause the smallest energy increase and the basin of attraction is locally widest. In two dimensions, time reversal and a coherent π rotation of such a homogeneous spin configuration yield the same transformation. Consequently, the ground state is only twofold degenerate, which corresponds simply to opposite orientations of magnetization [see Fig. 8(a)].

The low-energy metastable excitations can be obtained from the FM ground state by inverting the x components of all magnetic moments of a row of NPs, by inverting the y components of all magnetic moments of a column of NPs, or by doing both. Thus, the first metastable excited configuration shown in Fig. 8(b) is obtained by flipping, as described, the spins of one row or one column of NPs in a ferromagnetic ground state. Note that this is not a π spin reversal since one of the spin components remains essentially unchanged. Since the choice of the row or column is immaterial, one finds 12 such excited states for a given FM state. Starting from the other FM state or invoking time-inversion symmetry raises the total degeneracy of the first excited configuration to 24. The second excited state shown in Fig. 8(c) is obtained by flipping the spins of one row and one column of NPs. Again, the choice of the pair of row and column is immaterial. Taking into account time-inversion symmetry, this leads to 72 different degenerate configurations. The remaining low-energy excited states can be obtained in an analogous way by flipping the spins of additional rows or columns of NPs.

The fourfold degenerate antiferromagnetic state shown in Fig. 8(d) is a metastable LM of the rhombic ensemble provided that $1.27 < \alpha < \pi/2$. In particular, for $\alpha = 5\pi/12$ the excitation energy of this configuration is about three times larger than the first excitation energy [Fig. 8(b)]. As α is increased, and the rhombic lattice comes closer to the square lattice, the energy of the AF configuration decreases monotonously until at some point it becomes the ground state.

On the other hand, if one approaches the triangular lattice by decreasing α, the AF configuration becomes unstable. A sharp transition from a ferromagnetic to an antiferromagnetic ground state takes place at $\alpha_c \simeq 4\pi/9$. Other more complex noncollinear configurations have never been found to yield the lowest energy, at least for the considered small unit cell. While the limiting FM and AF ground-state configurations are expected, the observed sharp transition between them as a function of increasing α seems not obvious *a priori*. Furthermore, notice that the transition from FM to AF ground state occurs for an angle $\alpha = 4\pi/9$ which is rather close to the square lattice ($\alpha = \pi/2$). This shows that the FM configuration dominates most of the rhombic ground-state phase diagram.

A more detailed picture of the energy landscapes of rhombic dipole-coupled systems is provided by the kinetic network and disconnectivity graph shown in Fig. 9. The kinetic network consists of $N_{LM} = 198$ local minima or nodes and $N_{TS} = 1422$ transition states or edges. The segments highlighted in black correspond to the transitions connecting a LM to another one having a lower or equal energy and involving the smallest energy barrier. Physically, they represent the transitions that are most relevant in the stochastic dynamics [35]. One observes that the two ground states, indicated in red, are at the center of the network with the excited magnetic configurations being all funneled towards them. This becomes particularly clear if one focusses on the dynamically dominant transitions indicated by the black segments. Although the kinetic network as a whole is ergodic, in practice the dominant transitions show that the network tends to decompose in two inversion-symmetry-related subnetworks, each associated to the ground state that dominates it. This is a strong indication of a separation of timescales in the dynamics of the system, the relaxation being much faster within each subnetwork than between the subnetworks.

The average path distance $\langle d \rangle = 2.43$ of the kinetic network of rhombic magnetic NP arrangements with $\alpha = 5\pi/12$ is small. This means that most pairs of metastable states, however different in energy and configuration, can be connected by a small number of elementary LM-TS-LM transitions. As a matter of fact, the system needs to undergo only 1–2 elementary transitions to relax from most of the excited metastable states towards one of the ground states. This is a consequence of the extremely large local connectivity density $\rho_n = 0.48$ of the latter. Furthermore, the finite transitivity $C = 0.12$ shows the presence of a significant number of loops, which also contributes to avoid trapping. In sum, the KN of rhombic ensembles with $\alpha = 5\pi/12$ have small-world behavior, even
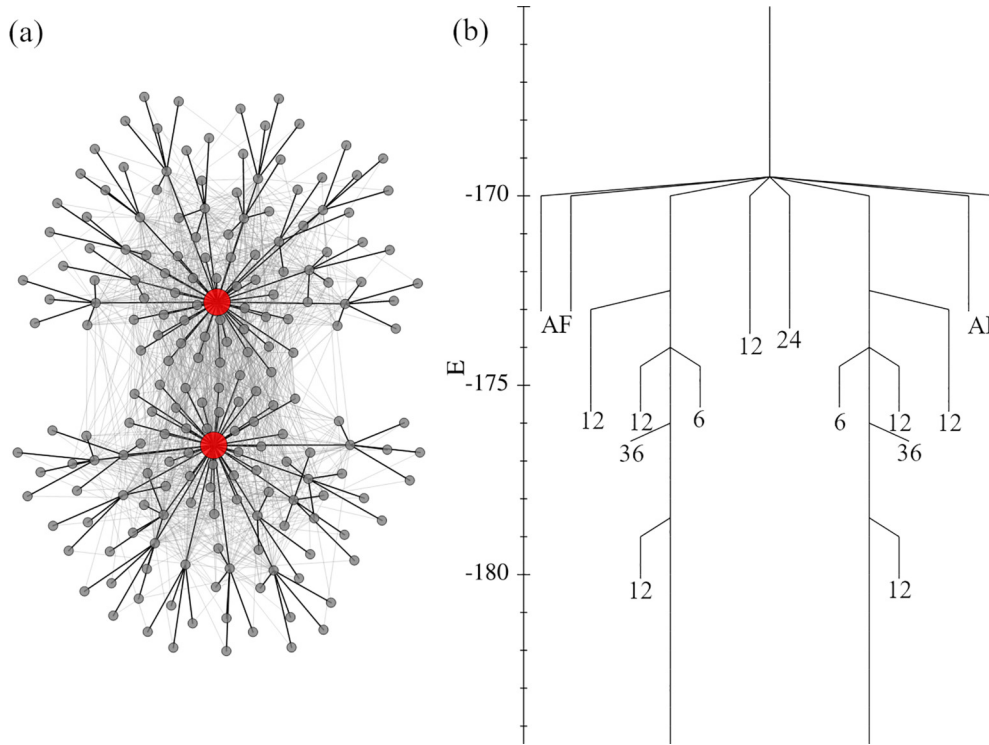
FIG. 9. (a) Kinetic network of local minima (nodes) and transition states (gray edges) and (b) disconnectivity graph of the energy landscape of a periodic rhombic lattice having $\alpha = 5\pi/12$ and $N = 36$ dipole-coupled magnetic moments in the unit cell (see also Fig. 8). In (a) the ferromagnetic ground states are indicated by the red circles. Furthermore, the edges in black highlight the downhill transition with the lowest-energy barriers. In (b) degenerate excited LM are grouped and the corresponding degeneracies are indicated.

though from a dynamical perspective it consists of two mostly independent subnetworks.

A complementary perspective to the ELs is provided by the disconnectivity graph shown in Fig. 9(b). One observes two clearly distinct funnels, which reflect the invariance of the energy upon reversal of all NP moments. Each ground state, lying at the bottom of the funnel, is surrounded by relatively large uphill energy barriers $\Delta E_\nearrow = 6.0$, which render them significantly more stable than any excited configuration. These two funnels correspond to the two subnetworks which were identified through the dominant transitions in the kinetic network of Fig. 9(a). The downhill energy barriers $\Delta E_\searrow$, i.e., the barriers encountered when going from an excited state towards the closest ground state are clearly smaller ($\Delta E_\searrow \simeq$ 1.5). For comparison, the energy barrier between the ground states is much larger [$\Delta E_0 = 14.9$, see Fig. 9(b)]. This implies that the relaxation between the subnetworks is comparatively much slower, in agreement with the previous analysis of the kinetic network.

The DG of the rhombic ensemble with $\alpha = 5\pi/12$ is an example of what is usually known as a double-funnel EL [61]. The large energy barrier between the two symmetric funnels might seem surprising since it is not observed in any of the limiting high-symmetry square ($\alpha = \pi/2$) and triangular ($\alpha = \pi/3$) ensembles between which the rhombic lattice interpolates. To clarify the origin of this behavior, it is useful to review some properties of the triangular lattice in more detail. We know that all in-plane ferromagnetic arrangements of the NP moments of a triangular lattice have the same energy, thus forming a continuously degenerate ground-state

manifold. However, despite having the same energy, the topography of the EL is not the same in the vicinity of different FM configurations. Configurations with comparatively small local curvatures, i.e., large spin-fluctuation entropies, are usually stabilized if the initial symmetry of the lattice is broken, whereas configurations with comparatively large local curvatures are destabilized [19,28]. In the case of a triangular lattice of dipole-coupled NPs one finds that the local curvatures are minimal (maximal) when the magnetization $\vec{\mu}$ points along the longer (shorter) diagonal of the lattice (see Fig. 1). Therefore, breaking the symmetry of the triangular arrangement, for instance, by distorting it into a rhombic lattice, generally leads to the stabilization (destabilization) of the FM configurations having $\vec{\mu}$ along the longer (shorter) diagonal of the lattice.

The C_6 symmetry of the triangular lattice is broken by a rhombic distortion. If the deviation from the triangular arrangement is is not too large ($\pi/3 < \alpha < 4\pi/9$) the ground state remains ferromagnetic but it is no longer continuously degenerate. In those cases one observes a continuous energy distribution of the collinear FM states depending on the orientation of the magnetization within the nanostructure plane. The width of the energy distribution, i.e., the energy difference ΔE_{FM} between the FM ground state and the least stable FM state, increases as the deviations $\delta\alpha = \alpha - \pi/3$ from the triangular lattice increases. For instance, $\Delta E_{FM} = 2.9$ for $\delta\alpha = \frac{1}{240}$ and $\Delta E_{FM} = 29.3$ for $\delta\alpha = \frac{1}{12}$. These changes in the behavior of the FM manifold as a function of α have interesting consequences. If $\delta\alpha > 0$ is very small, the energy barrier associated to a coherent rotation of $\vec{\mu}$, keeping the FM order, remains small. Therefore, direct transitions between the two

ground states having opposite orientations of the NP moments $\vec{\mu}$ are possible within the FM manifold. This results in extremely funneled disconnectivity graphs in agreement with the behavior observed for the perfect and weakly disordered triangular lattices [35,36]. However, as $\delta\alpha$ further increases, the coherent-rotation mechanism becomes energetically very disadvantageous because of the drastic increase of ΔE_{FM}. Other transition mechanisms become then much more important. In the case of the rhombic ensemble with $\alpha = 5\pi/12$ ($\delta\alpha = \frac{1}{12}$) shown in Fig. 8, magnetic rearrangements involving multiple noncollinear transition states and intermediate local minima yield the most efficient pathways for the transition between the FM ground states. However, these MEPs involve multiple elementary transitions with significant energy barriers. This explains the double-funnel EL observed in Fig. 9. Results on rhombic ensembles having larger unit cells ($N = 64$ and 100) indicate that the energy barrier between the two funnels increases approximately linearly as a function of the system size N. Therefore, ergodicity breaking seems most plausible in the thermodynamic limit, where the separating energy barrier cannot be overcome on experimental timescales.

Hitherto, the discussion has revolved around rhombic ensembles with a FM ground state, which holds for $\pi/3 < \alpha < 4\pi/9$. Rhombic ensembles with $4\pi/9 \leqslant \alpha < \pi/2$ have AF ground states. Some important qualitative differences between these two types of ensembles are related to the contrasting symmetry and degeneracy of their ground states. In the case of a FM ground state, the degeneracy is twofold, corresponding to states having opposite magnetization directions along the longer diagonal of the rhombic lattice. In contrast, in the case of an AF ground state, the degeneracy is fourfold since the alternating chains of magnetic moments may be aligned along the x or y directions (see Figs. 6). A direct consequence of the higher fourfold symmetry of the AF order is that the energy barriers associated to transitions in AF ensembles are much smaller than in the FM case since the angle between equivalent stable magnetization directions (easy axes) in the AF case is half of the value in the FM case. In fact, the largest energy barrier between AF ground states $\Delta E_{AF}^{max} = 1.4$, found for $\alpha = 4\pi/9$, is an order of magnitude smaller than the largest barrier observed for FM ground states $\Delta E_{FM}^{max} = 29.3$. It follows that a coherent rotation is the most efficient transition mechanism between the fourfold-degenerate AF ground states, even for $\alpha = 4\pi/9$, where the highest AF energy barriers are found. Similar symmetry-related trends are known to apply to magnetocrystalline anisotropies where, for example, uniaxial anisotropies are usually much larger than cubic anisotropies [62].

E. Oblique lattice

The least symmetric Bravais lattice in two dimensions is the oblique lattice, which is defined by $\alpha \neq \pi/2$ and $\lambda_x \neq \lambda_y$ (see Fig. 1). Its local symmetries are reduced to the C_2 point group and time inversion. In this section we focus on lattices having α and λ_x/λ_y significantly different from $\pi/2$ and 1, respectively, since these limits correspond to the rectangular and rhombic lattices which have been discussed in detail in Secs. III C and III D. Specifically, we consider an oblique lattice having $\alpha = 7\pi/18$ and $\lambda_x/\lambda_y = 1.05$,

which are representative of a wide range of oblique-lattice ensembles.

In Fig. 10, the ground-state magnetic configuration and the first and second excited configurations are shown. In all cases the magnetic moments form head-to-tail chains along the y direction, which has the shortest NN distance. A very similar behavior has been observed in rectangular lattices (Sec. III C). However, notice that in the present oblique lattice the ground state is ferromagnetic in contrast to the AF arrangement of spin chains found in rectangular ensembles [cf. Figs. 6(a) and 10(a)]. Whether the ground state of the oblique lattice is ferromagnetic or antiferromagnetic depends in fact on the angle α. Smaller α, closer to the triangular lattice, yield FM order whereas larger α, closer to the rectangular lattice, yield AF order. The actual transition from FM to AF ground state occurs at $\alpha_c \simeq 4\pi/9$, a value that is quite similar to the one observed in rhombic ensembles (Sec. III D). According to our calculations, α_c is nearly independent of the NN-distance ratio for $\lambda_x/\lambda_y \in [1.0, 1.3]$.

The metastable configurations are obtained from the ground state by flipping the orientation of chains of magnetic moments along the y direction. For instance, the first excited state is obtained by flipping one of the spin chains of the FM ground state and the second excited state is obtained by flipping a second chain beside the first one [cf. Figs. 10(a)–10(c)]. Since flipping the chains breaks the periodicity of the ground state along the x direction, and taking into account the boundary condition, six degenerate magnetic configurations are obtained through translations. Including time inversion the degeneracy of the first and second excited states is raised to 12. As already observed for rectangular ensembles in Sec. III C, all metastable states of the considered oblique lattice can be obtained by flipping additional chains of magnetic moments along the y direction. This behavior has been found in all oblique ensembles having $\lambda_x/\lambda_y \geqslant 1.05$. Hence, as in the rectangular lattice, the chains of head-to-tail moments can be treated as Ising spins pointing along the $\hat{y} = (\cos\alpha, \sin\alpha, 0)$ or $-\hat{y}$ directions. Since we have $L = 6$ chains in the unit cell ($N = 36$) the total number of LM is $N_{LM} = 2^L = 64$.

Figure 11(a) shows the kinetic network of the oblique lattice illustrated in Fig. 10. It consists of 64 nodes, representing the LM, and 192 edges, representing the transitions across first-order saddle points. Each LM is connected to exactly six other LM, which are obtained by flipping a spin chain along the y direction on the considered configuration. This results in a latticelike KN, which is identical to the one obtained for the rectangular lattice [cf. Figs. 7(a) and 11(a)]. Consequently, most of the considerations made in this context for rectangular ensembles apply straightforwardly to oblique ensembles. In short, the relaxation dynamics can be pictured as the succession of largely uncorrelated flips of spin chains. The KN is bipartite ($C = 0$) and without hubs. All nodes have the same degree density $\rho_n = 0.1$. Together with the comparatively large average path distance $\langle d \rangle = 3.1$, one concludes that oblique-lattice NP ensembles are not good structure seekers. Moreover, their KNs do not exhibit small-world behavior.

The corresponding DG, shown in Fig. 11(b), is also very similar to the one obtained for the rectangular system [cf. Figs. 7(b) and 11(b)]. All metastable states are remarkably
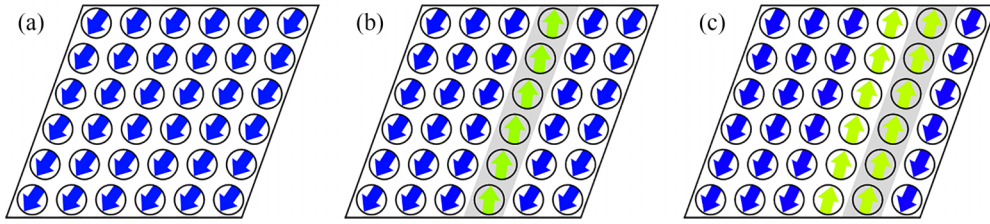
FIG. 10. Magnetic configurations of (a) the ground state, (b) the first excited state, and (c) the second excited state of an oblique-lattice ensemble having $N = 36$ magnetic moments in the unit cell with periodic boundary conditions. The ratio between the NN distances is $\lambda_x/\lambda_y = 1.05$ and the angle between the Bravais vectors is $\alpha = 7\pi/18$. See Fig. 1.

stable. They are clearly separated from the other LM by energy barriers that are much larger than the energy differences between the connected configurations. Furthermore, a clear energy hierarchy exists between the ground states and the various groups excited states. In sum, the DG has all the main features of the so-called willow-tree graph [57]. Such systems are expected to be good structure seekers as soon as $k_B T$ is of the order of the characteristic energy barriers [57,59,60]. However, as in the rectangular case, one has to keep in mind that the average number of elementary transitions required to relax from an arbitrary magnetic configuration towards the ground state increases linearly with increasing unit-cell size. This is a consequence of the lattice nature of the KN. Therefore, it is not obvious at this point whether such a system would be a good structure seeker in the thermodynamic limit.

The physical behavior of oblique ensembles as a function of α and λ_x/λ_y can be clarified by referring to the Ising model given by Eq. (6). In this model, the interaction between the chains of magnetic moments is characterized by the coupling constant J, where $J > 0$ ($J < 0$) corresponds to antiferromagnetic (ferromagnetic) ground-state order. Let us analyze the dependence of J on α, keeping $\lambda_x/\lambda_y = 1.05$ fixed, by starting with the above-discussed oblique lattice ($\alpha = 7\pi/18 \simeq 1.22$) for which $J = -1.4$ gives a very good fit of the LM energies. In this case the ground state is FM and the energy differences between the different groups of excited states are significant [see Fig. 11(b)]. As α is increased, the absolute value of J decreases and the FM order becomes less stable. For instance, for $\alpha \simeq 1.34$ we find $J = -0.2$. Accordingly, the energy differences between the metastable states become significantly smaller. A transition takes place at $\alpha_c \simeq 1.37$, where the sign of J changes and the ground state switches from ferromagnetic to antiferromagnetic order. Close to the transition, the energy differences between the metastable states remain very small and in particular the AF ground state is not very stable. However, as α is further increased, J and the energy differences between the metastable states grow. Finally, for $\alpha = \pi/2$, in the rectangular lattice, the maximum positive value of $J \simeq 1.25$ is reached.
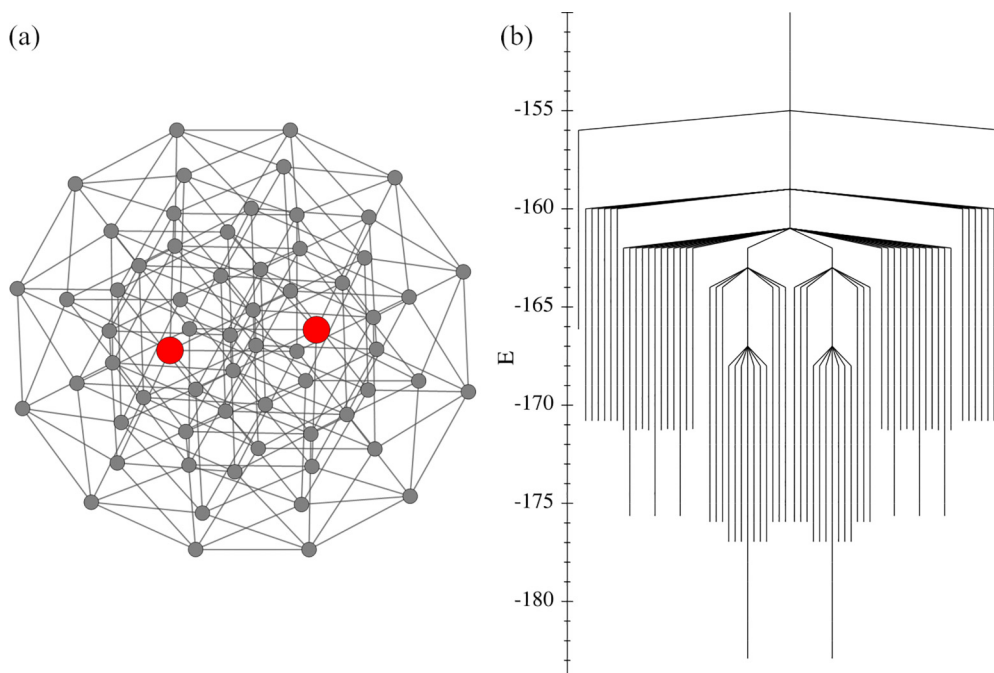

FIG. 11. (a) Kinetic network of local minima (nodes) and transition states (edges) and (b) disconnectivity graph of the energy landscape of a periodic oblique lattice having $\lambda_x/\lambda_y = 1.05$, $\alpha = 7\pi/18$, and $N = 36$ dipole-coupled magnetic moments in the unit cell. In (a) the ground-state nodes are highlighted in red. See also Figs. 1 and 10.

Concerning the dependence of J on the NN-distance ratio λ_x/λ_y, the same reasoning as for the rectangular lattice applies. Increasing λ_x/λ_y weakens the coupling J between neighboring chains irrespectively of α since the distance between the chains increases. This reduction of $|J|$ manifests itself as a decrease of the energy differences between the metastable states, which are primarily conditioned by this coupling. Finally, in the limit $\lambda_x/\lambda_y \gg 1$, J tends to zero and the chains of magnetic moments decouple.

IV. CONCLUSION

The energy landscapes of two-dimensional ensembles of dipole-coupled magnetic nanoparticles have been investigated for the five different two-dimensional Bravais lattices, namely, square, triangular, rectangular, rhombic, and oblique lattices. The corresponding ergodic networks of local minima and connecting transition states have been characterized. The analysis shows that the underlying lattice structure has a most profound influence on these physical behavior of these magnetic nanostructures. Square and triangular lattices are found to be extremely good structure seekers. In this case almost any magnetic configurations being directly connected to the continuously degenerate ground state. The kinetic networks are starlike and show small-world behavior. The corresponding disconnectivity graphs resemble palm trees [48]. Rhombic ensembles, in contrast, have double-funnel energy landscapes with two saturated ferromagnetic ground states whose magnetization points in opposite directions. They lie at the bottom of distinct funnels separated by a large energy barrier, which grows linearly with unit-cell size N. Hence, ergodicity breaking is expected in the thermodynamic limit. Finally, it was shown that rectangular and oblique ensembles behave very much like a one-dimensional chain of Ising spins. The results for the KNs and DGs reflect complementary aspects of their ELs. The KNs suggest that these systems are not efficient structure seekers since the number of elementary LM-TS-LM transitions required to connect different metastable configurations with each other, or with the ground states, are relatively large. Nevertheless, the DGs resemble willow trees with quite asymmetric energy profiles, the downward barriers being significantly smaller than the upward ones, which generally favors unhindered relaxation once $k_B T$ becomes comparable to the characteristic energy barriers. A detailed size-scaling analysis would be necessary in order to elucidate their behavior in the thermodynamic limit.

The present investigations have allowed us to identify a number of characteristics of the energy landscapes of two-dimensional ensembles of interacting magnetic NPs and in particular to reveal the remarkable profound dependence of the collective behavior on the underlying structural arrangement of the nanostructure. A detailed description of the actual relaxation dynamics for different experimentally relevant initial conditions (e.g., high-field saturation, zero-field quenching, etc.) seems therefore most worthwhile. This can be done by taking advantage of the discretization of the configurational space in the attraction basins associated to the different LM and by following the time evolution of the statistical distribution of the system among them in the framework of a master equation (Markovian hypothesis). The central transition rates can be estimated by applying transition-state theory to coupled LLG equations as proposed in Ref. [63]. The Markovian dynamics of disordered ensembles of magnetic NPs have already been investigated in this way [35,36]. In particular for highly symmetric lattice structures showing a continuously degenerate ground state, attention should be paid to the contribution of fluctuations of the magnetic configuration in the directions perpendicular to the constant-energy curves. These tend to favor specific magnetic configuration within the ground-state manifold and therefore are expected to significantly affect the dynamics at low temperatures [19,28].

The primary focus of this paper resides on the dipole-dipole interaction between magnetic nanoparticles in two dimensions. In view of more comprehensive comparisons with experiment, it would be worthwhile to extend the present investigations by taking other magnetic effects into account. This includes, for instance, local energy contributions, such as the magnetocrystalline and shape anisotropies of individual NPs, a more detailed description of the interactions including higher-order multipole moment contributions, which are known to be important if the NPs are not spherical, as well as the coupling of the NP moments to external magnetic fields [64]. Further interesting research directions to be pursued in the present framework would be to investigate three-dimensional nanostructures and to include other types of interactions, such as exchange and Ruderman-Kittel-Kasuya-Yosida (RKKY) couplings, which play an important role in spin glasses [65,66].

[1] C. Nisoli, R. Moessner, and P. Schiffer, Colloquium: Artificial spin ice: Designing and imaging magnetic frustration, Rev. Mod. Phys. **85**, 1473 (2013).

[2] A. Farhan, P. M. Derlet, A. Kleibert, A. Balan, R. V. Chopdekar, M. Wyss, J. Perron, A. Scholl, F. Nolting, and L. J. Heyderman, Direct Observation of Thermal Relaxation in Artificial Spin Ice, Phys. Rev. Lett. **111**, 057204 (2013).

[3] L. Anghinolfi, H. Luetkens, J. Perron, M. G. Flokstra, O. Sendetskyi, A. Suter, T. Prokscha, P. M. Derlet, S. Lee, and L. J. Heyderman, Thermodynamic phase transitions in a frustrated magnetic metamaterial, Nat. Commun. **6**, 8278 (2015).

[4] E. Östman, H. Stopfel, I.-A. Chioar, U. B. Arnalds, A. Stein, V. Kapaklis, and B. Hjörvarsson, Interaction modifiers in artificial spin ices, Nat. Phys. **14**, 375 (2018).

[5] R. Streubel, N. Kent, S. Dhuey, A. Scholl, S. D. Kevan, and P. Fischer, Spatial and temporal correlations of XY macro spins, Nano Lett. **18**, 7428 (2018).

[6] N. A. Frey and S. Sun, Magnetic nanoparticle for information storage applications, in *Inorganic Nanoparticles: Synthesis, Applications, and Perspectives*, edited by C. Altavilla and E. Ciliberto (CRC Press, Boca Raton, FL, 2010), Chap. 2, pp. 33–68.

[7] S. Karmakar, S. Kumar, R. Rinaldi, and G. Maruccio, Nanoelectronics and spintronics with nanoparticles, J. Phys.: Conf. Ser. **292**, 012002 (2011).

[8] B. Dieny, I. L. Prejbeanu, K. Garello, P. Gambardella, P. Freitas, R. Lehndorff, W. Raberg, U. Ebels, S. O. Demokritov, J. Akerman, A. Deac, P. Pirro, C. Adelmann, A. Anane, A. V. Chumak, A. Hirohata, S. Mangin, S. O. Valenzuela, M. C. Onbaşlı, M. d'Aquino *et al.*, Opportunities and challenges for spintronics in the microelectronics industry, Nat. Electron. **3**, 446 (2020).

[9] K. Lee, J. Callaway, and S. Dhar, Electronic structure of small iron clusters, Phys. Rev. B **30**, 1724 (1984).

[10] K. Lee, J. Callaway, K. Kwong, R. Tang, and A. Ziegler, Electronic structure of small clusters of nickel and iron, Phys. Rev. B **31**, 1796 (1985).

[11] I. M. L. Billas, J. A. Becker, A. Chatelain, and W. A. de Heer, Magnetic Moments of Iron Clusters with 25 to 700 Atoms and Their Dependence on Temperature, Phys. Rev. Lett. **71**, 4067 (1993).

[12] J. P. Bucher, D. C. Douglass, and L. A. Bloomfield, Magnetic Properties of Free Cobalt Clusters, Phys. Rev. Lett. **66**, 3052 (1991).

[13] R. A. Guirado-Lopez, J. Dorantes-Davila, and G. M. Pastor, Orbital Magnetism in Transition-Metal Clusters: From Hund's Rules to Bulk Quenching, Phys. Rev. Lett. **90**, 226402 (2003).

[14] G. M. Pastor, J. Dorantes-Davila, and K. H. Bennemann, Size and structural dependence of the magnetic properties of small 3d-transition-metal clusters, Phys. Rev. B **40**, 7642 (1989).

[15] G. M. Pastor, J. Dorantes-Davila, S. Pick, and H. Dreysse, Magnetic Anisotropy of $3d$ Transition-Metal Clusters, Phys. Rev. Lett. **75**, 326 (1995).

[16] M. Muñoz-Navia, J. Dorantes-Dávila, D. Zitoun, C. Amiens, N. Jaouen, A. Rogalev, M. Respaud, and G. M. Pastor, Tailoring the magnetic anisotropy in CoRh nanoalloys, Appl. Phys. Lett. **95**, 233107 (2009).

[17] D. C. Douglass, A. J. Cox, J. P. Bucher, and L. A. Bloomfield, Magnetic properties of free cobalt and gadolinium clusters, Phys. Rev. B **47**, 12874 (1993).

[18] W. A. de Heer, P. Milani, and A. Chatelain, Spin Relaxation in Small Free Iron Clusters, Phys. Rev. Lett. **65**, 488 (1990).

[19] D. Schildknecht, L. J. Heyderman, and P. M. Derlet, Phase diagram of dipolar-coupled XY moments on disordered square lattices, Phys. Rev. B **98**, 064420 (2018).

[20] S. K. Baek, P. Minnhagen, and B. J. Kim, Kosterlitz-Thouless transition of magnetic dipoles on the two-dimensional plane, Phys. Rev. B **83**, 184409 (2011).

[21] B. Alkadour, J. I. Mercer, J. P. Whitehead, B. W. Southern, and J. van Lierop, Dipolar ferromagnetism in three-dimensional superlattices of nanoparticles, Phys. Rev. B **95**, 214407 (2017).

[22] M. Varón, M. Beleggia, T. Kasama, R. J. Harrison, R. E. Dunin-Borkowski, V. F. Puntes, and C. Frandsen, Dipolar magnetism in ordered and disordered low-dimensional nanoparticle assemblies, Sci. Rep. **3**, 1234 (2013).

[23] P. Torche, C. Munoz-Menendez, D. Serantes, D. Baldomir, K. L. Livesey, O. Chubykalo-Fesenko, S. Ruta, R. Chantrell, and O. Hovorka, Thermodynamics of interacting magnetic nanoparticles, Phys. Rev. B **101**, 224429 (2020).

[24] E. H. Sánchez, M. Vasilakaki, S. S. Lee, P. S. Normile, M. S. Andersson, R. Mathieu, A. López-Ortega, B. P. Pichon, D. Peddis, C. Binns, P. Nordblad, K. Trohidou, J. Nogués, and J. A. D. Toro, Crossover from individual to collective magnetism in dense nanoparticle systems: Local anisotropy versus dipolar interactions, Small **18**, 2106762 (2022).

[25] P. J. Jensen and G. M. Pastor, Dipole coupling induced magnetic ordering in an ensemble of nanostructured islands, Phys. Status Solidi A **189**, 527 (2002).

[26] P. J. Jensen and G. M. Pastor, Low-energy properties of two-dimensional magnetic nanostructures: Interparticle interactions and disorder effects, New J. Phys. **5**, 68 (2003).

[27] G. M. Pastor and P. J. Jensen, Elementary transitions and magnetic correlations in two-dimensional disordered nanoparticle ensemble, Phys. Rev. B **78**, 134419 (2008).

[28] S. Prakash and C. L. Henley, Ordering due to disorder in dipolar magnets on two-dimensional lattices, Phys. Rev. B **42**, 6574 (1990).

[29] P. Politi, M. G. Pini, and R. L. Stamps, Dipolar ground state of planar spins on triangular lattices, Phys. Rev. B **73**, 020405(R) (2006).

[30] D. Schildknecht, M. Schütt, L. J. Heyderman, and P. M. Derlet, Continuous ground-state degeneracy of classical dipoles on regular lattices, Phys. Rev. B **100**, 014426 (2019).

[31] T. Jonsson, J. Mattsson, C. Djurberg, F. A. Khan, P. Nordblad, and P. Svedlindh, Aging in a Magnetic Particle System, Phys. Rev. Lett. **75**, 4138 (1995).

[32] M. Sasaki, P. E. Jönsson, H. Takayama, and H. Mamiya, Aging and memory effects in superparamagnets and superspin glasses, Phys. Rev. B **71**, 104405 (2005).

[33] D. Parker, V. Dupuis, F. Ladieu, J.-P. Bouchaud, E. Dubois, R. Perzynski, and E. Vincent, Spin-glass behavior in an interacting γ-Fe$_2$O$_3$ nanoparticle system, Phys. Rev. B **77**, 104428 (2008).

[34] M. Vasilakaki, G. Margaris, D. Peddis, R. Mathieu, N. Yaacoub, D. Fiorani, and K. Trohidou, Monte Carlo study of the superspin glass behavior of interacting ultrasmall ferrimagnetic nanoparticles, Phys. Rev. B **97**, 094413 (2018).

[35] D. Gallina and G. M. Pastor, Disorder-Induced Transformation of the Energy Landscapes and Magnetization Dynamics in Two-Dimensional Ensembles of Dipole-Coupled Magnetic Nanoparticles, Phys. Rev. X **10**, 021068 (2020).

[36] D. Gallina and G. M. Pastor, Structural disorder and collective behavior of two-dimensional magnetic nanostructures, Nanomaterials **11**, 1392 (2021).

[37] J. P. K. Doye and D. J. Wales, The effect of the range of the potential on the structure and stability of simple liquids: from clusters to bulk, from sodium to C$_{60}$, J. Phys. B: At., Mol. Opt. Phys. **29**, 4859 (1996).

[38] O. M. Becker and M. Karplus, The topology of multidimensional potential energy surfaces: Theory and application to peptide structure and kinetics, J. Chem. Phys. **106**, 1495 (1997).

[39] L. J. Munro and D. J. Wales, Defect migration in crystalline silicon, Phys. Rev. B **59**, 3969 (1999).

[40] D. J. Wales, *Energy Landscapes: Applications to Clusters, Biomolecules and Glasses* (Cambridge University Press, Cambridge, 2004).

[41] M. A. Miller, J. P. K. Doye, and D. J. Wales, Structural relaxation in Morse clusters: Energy landscapes, J. Chem. Phys. **110**, 328 (1999).

[42] J. Nocedal, Updating quasi-newton matrices with limited storage, Math. Comput. **35**, 773 (1980).

[43] J. C. Mauro, R. J. Loucks, and J. Balakrishnan, A simplified eigenvector-following technique for locating transition points in an energy landscape, J. Phys. Chem. A **109**, 9578 (2005).

[44] R. D. Luce and A. D. Perry, A method of matrix analysis of group structure, Psychometrika **14**, 95 (1949).

[45] M. E. J. Newman, *Networks* (Oxford University Press, Oxford, 2010).

[46] A. L. Barabási, *Network Science* (Cambridge University Press, Cambridge, 2016).

[47] D. J. Watts and S. H. Strogatz, Collective dynamics of 'small-world' networks, Nature (London) **393**, 440 (1998).

[48] D. J. Wales, M. A. Miller, and T. R. Walsh, Archetypal energy landscapes, Nature (London) **394**, 758 (1998).

[49] J. Villain, R. Bidaux, J.-P. Carton, and R. Conte, Order as an effect of disorder, J. Phys. (France) **41**, 1263 (1980).

[50] P. A. McClarty, P. Stasiak, and M. J. P. Gingras, Order-by-disorder in the XY pyrochlore antiferromagnet, Phys. Rev. B **89**, 024425 (2014).

[51] C. L. Henley, Ordering Due to Disorder in a Frustrated Vector Antiferromagnet, Phys. Rev. Lett. **62**, 2056 (1989).

[52] F. Harary, *Graph Theory* (CRC Press, Boca Raton, FL, 1969).

[53] D. J. Wales and T. V. Bogdan, Potential energy and free energy landscapes, J. Phys. Chem. B **110**, 20765 (2006).

[54] D. Mehta, C. Hughes, M. Schröck, and D. J. Wales, Potential energy landscapes for the 2D XY model: Minima, transition states, and pathways, J. Chem. Phys. **139**, 194503 (2013).

[55] D. Mehta, C. Hughes, M. Kastner, and D. J. Wales, Potential energy landscape of the two-dimensional XY model: Higher-index stationary points, J. Chem. Phys. **140**, 224503 (2014).

[56] J. W. R. Morgan, D. Mehta, and D. J. Wales, Properties of kinetic transition networks for atomic clusters and glassy solids, Phys. Chem. Chem. Phys. **19**, 25498 (2017).

[57] T. R. Walsh and D. J. Wales, Relaxation dynamics of C_{60}, J. Chem. Phys. **109**, 6691 (1998).

[58] C. Xu and G. E. Scuseria, Tight-Binding Molecular Dynamics Simulations of Fullerene Annealing and Fragmentation, Phys. Rev. Lett. **72**, 669 (1994).

[59] X. Liu, D. J. Klein, and W. A. Seitz, Sixty-atom carbon cages, J. Comput. Chem. **12**, 1265 (1991).

[60] D. E. Manolopoulos, J. C. May, and S. E. Down, Theoretical studies of the fullerenes: C_{34} to C_{60}, Chem. Phys. Lett. **181**, 105 (1991).

[61] J. P. K. Doye, M. A. Miller, and D. J. Wales, The double-funnel energy landscape of the 38-atom Lennard-Jones cluster, J. Chem. Phys. **110**, 6896 (1999).

[62] B. D. Cullity, *Introduction to Magnetic Materials* (Addison-Wesley, Reading, MA, 2008).

[63] P. F. Bessarab, V. M. Uzdin, and H. Jonsson, Harmonic transition-state theory of thermal spin transitions, Phys. Rev. B **85**, 184409 (2012).

[64] E. Y. Vedmedenko, N. Mikuszeit, H. P. Oepen, and R. Wiesendanger, Multipolar Ordering and Magnetization Reversal in Two-Dimensional Nanomagnet Arrays, Phys. Rev. Lett. **95**, 207202 (2005).

[65] K. Binder and A. P. Young, Spin glasses: Experimental facts, theoretical concepts, and open questions, Rev. Mod. Phys. **58**, 801 (1986).

[66] S. F. Edwards and P. W. Anderson, Theory of spin glasses, J. Phys. F: Met. Phys. **5**, 965 (1975).